Deep Learning Based Segmentation Of The Posterior Eye To Study Glaucoma and Age Related Morphological Changes

Submitted by: Ahmad Madhwala, Biomedical Engineering

Advisor: Dr. Jun Liu, Ph.D., Biomedical Engineering

April 7, 2024

Abstract

Glaucoma, the leading cause of irreversible blindness in the United States, poses therapeutic challenges with current methods relying on IOP (intraocular pressure) management. However, even after effective lowering of IOP, patients sometimes can still lose vision permanently. Recent studies highlight the potential association between peripapillary sclera (PPS) and lamina cribrosa (LC) biomechanical properties and glaucoma risk. This study aims to explore morphological differences in posterior ocular tissues in order to understand more effective alternatives of focusing treatments for glaucoma.

This study utilized a 50 MHz Vivo 2100 ultrasound imaging system for posterior eye assessment using both healthy and glaucomatous human donor eyes. A portion of the ultrasound images were processed and manually segmented using a custom software. Using this segmented data, a DeepLab V3+ DL-based auto-segmentation tool was employed with a Timm-Efficient Net encoder was trained on for more efficient and streamlined segmentation of the remaining data set. The DL model demonstrated good accuracy in auto-segmentation, surpassing 90% accuracy in relevant ocular tissue layers. Morphological data consisting of the thickness of the retina, sclera, and LC as well as depth between the Bruch's membrane opening (BMO) and anterior LC were calculated in MatLab. Our results showed a significant difference in thickness between healthy and glaucoma eyes in the retina and age-related thinning of the PPS demonstrating the potential of DL-based auto-segmentation for ocular tissue morphological assessment in glaucoma therapeutics.

Acknowledgements

I would like to express my deepest gratitude to my professor and advisor, Dr. Jun Liu, for her invaluable guidance and feedback, and to my committee member Dr. Rizwan Ahmad. I would also like to give special thanks my mentor Zihao Chen, for his continued support. Lastly, I would like to thank Lia Gomez-Perez and Dr. Sunny Kwok, and the other students in Dr. Liu's lab for their help throughout this project.

1. Table of Contents

2. List of Figures 4

3. List of Tables 4

4. Introduction 5

4.1. Background 5

4.2. Significance 6

4.3. Research Goals 6

5. Methodology 7

5.1 Aim 1- Segmentation and model training 7

5.2. Aim 2: Calculating morphological properties using segmented data..... 12

6. Results & Discussion 14

7. Conclusions & Future Work 17

2. List of Figures

Figure 1 Diagram of how increased IOP can cause damage to eye ……..…… **5**

Figure 2 Vivo2100 Imaging set up for ultrasound scan acquisition of donor eyes ……..…….. **7**

Figure 3 Depiction of converting B-mode images to radial frames …….. **8**

Figure 4 Fully segmented radial frame ……. **9**

Figure 5 Deep Learning model architecture of DeepLabV3+ …… **10**

Figure 6 Segmented Radial Image and corresponding multiclass mask (left) and model output prediction of each layer class ……..…….. **11**

Figure 7 Model performance metrics calculations …….. **12**

Figure 8 Depiction of how morphological properties were calculated …….…….. **13**

Figure 9 Bar graph between all healthy and glaucoma tissue thicknesses (left) and healthy and glaucoma retinal thickness (right) ……...……. **15**

Figure 10 Thickness of PPS with age using axial thickness scatter (top left) and average per age group (top right) and the Euclidean thickness scatter (bottom left) and average per age group (bottom right) ……..…….. **15**

Figure 11 Bar graph of mean BMO to anterior LC depth for healthy and glaucoma ……....… **16**

3. List of Tables

Table 1 Patient demographics of all donor eyes used in study ……..… **8**

Table 2 Patient demographics of all donor eyes used in DL model training …….....…. **12**

Table 3 DL model performance with optimized alpha regularization value …….……. **14**

4. Introduction

4.1 Background

Glaucoma is the leading cause of irreversible blindness worldwide affecting roughly 3 million Americans and over 70 million people worldwide [2]. It is estimated that roughly 50% of true glaucoma patients remain undiagnosed [2]. This disease is comprised of a set of optic neuropathies resulting from progressive retinal ganglion cell (RGC) deterioration and damage of the optic nerve head (ONH) [5]. It is widely accepted that one of the leading causes of

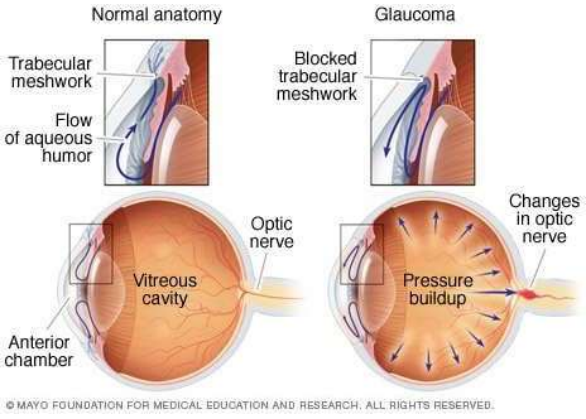

Figure 1: How Glaucoma Affects Eye

glaucoma is the increase in intraocular pressure (IOP) due to improper drainage of the Aqueous Humor [15]. As a result, this pressure builds up and begins to damage the optic nerve head (ONH) leading to vision loss and irreversible blindness [1,2,3].

However, glaucoma is a slow progressing disease and often takes 10-15 years to fully cause blindness [3]. In fact, many patients with primary open angle glaucoma (POAG) do not experience elevated IOP levels and have levels <22 mmHg [16]. For this reason, early diagnosis and monitoring of risk factors is essential to prevent irreversible damage to the eye. Some common risk factors include older age, family history of glaucoma, black race, use of corticosteroids, and high intraocular pressure [5,8]. Additionally, recent work demonstrates that

biomechanical properties of the posterior tissue layers including the retina, peripapillary sclera (PPS), and lamina cribrosa (LC) could also be linked with increased glaucoma risk [12, 13]. The LC is a membrane that allows the nerve fibers to transmit sensory information and is often the main site of damage in glaucoma and its severe deformations may increase the risk of onset of glaucoma. Hence, this study aims to investigate morphological related effects of these ocular tissues to explore alternative methods of glaucoma diagnosis allowing clinicians to better manage the disease and begin early treatment before irreversible damage begins. The goal of this project is to focus on thickness related morphologies in the major anatomical features in the posterior eye including Sclera, Retina, and Lamina Cribrosa (LC).

4.2 Significance

Glaucoma is a slow progressing disease that can permanently affect people's vision for life. Further studies of morphological changes in tissue are important as this may lead to alternative and more efficient diagnosis for this disease. Further research is needed regarding what morphological and biomechanical properties can be used by clinicians as systematic risk factors for early glaucoma. Deep Learning models may help automatically segment ultrasonic images to calculate these morphological properties and provide insights on some of the properties that are different between healthy and glaucoma patients. Thus, this study lays the foundation behind a predictive tool to assist in management of glaucoma progression.

4.3 Research Goals

There are two main objectives of this research project. The first is to manually segment out the relevant ocular layers in previously acquired ultrasound images in several donor eyes. Using this

segmented data, a deep learning model was trained and used to automate the segmentation process of the remaining eyes in the data set. The second aim is to use the segmented data to make calculations regarding the thickness of the layers and use statistical analysis to determine any major differences between the healthy and glaucoma eyes.

5. Methodology

5.1 Aim 1- Segmentation and model training

Ex vivo ultrasound imaging protocol for posterior eye

Ex vivo ultrasound scans were previously collected from human donor eyes (n = 37). All eyes were stored in saline solution at room temperature and all scans were taken within 48 hours postmortem. 37 donor globes were scanned laterally using the Vevo2100 50 MHz system (MS700 probe, Vevo 2100, FujiFilm VisualSonics, Inc., Toronto, Canada) in the nasal to temporal direction on an anti-vibration table to reduce noise. 307 B-Mode slice images were acquired and were stored as image packages for each eye.

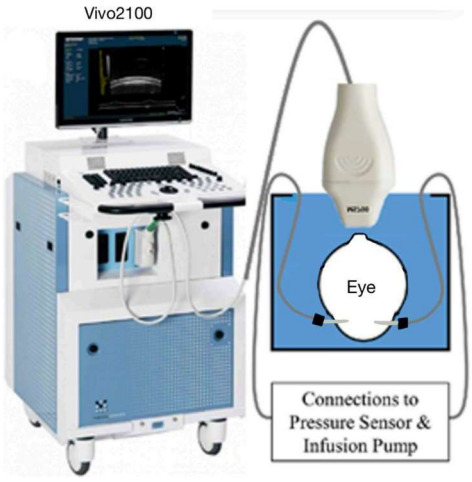

Figure 2: Ultrasound Vivo Imaging System and Setup

Right Eyes	21
Left Eyes	16
Male	15
Female	20
Healthy	28
Glaucoma	7
African American	7
Caucasian	28
Age Range	20-80
Age Mean	59.3

Table 1: Patient Demographics Of Donor Eyes (n=37)

Image processing and segmentation

Once the image data was acquired, the packages were processed and uploaded to the lab custom software for segmentation. Our custom software automatically converts the laterally stacked image packages into rotational images about the ONH which makes each frame a specific rotational degree (0-360 in 4.5 degree increments, n = 80) which makes the segmentation easier and more consistent when later used for DL training. This is because not all B-mode images have equal amounts of data as the ones near the center contain the LC and ONH. Converting to radial frames ensures consistency among images in terms geometry and visualization.

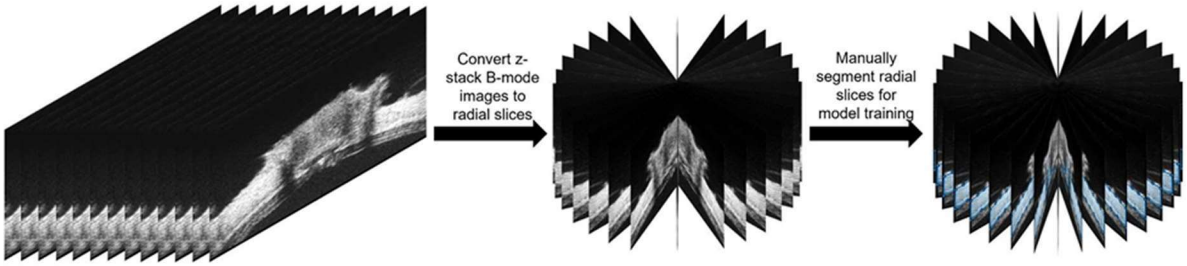

Figure 3: Lateral To Radial Image Resliced

The specific anatomical features and or layers of interest are the Posterior Sclera Boundary (left and right), Anterior Sclera Boundary (left and right), Neural Boundary (left and right), Internal

limiting membrane, Bruch's Membrane Opening (BMO), and Anterior/Posterior LC. The left and right sides of the sclera are separated due to the opening created by the ONH **(figure 4).** A simplified segmentation model was used in which the ONH was fully extruded following the vertical white boundaries in order to create fully connected 2D regions. Our software saves segmented data points as 3-D cloud points and the data is formatted in X, Y, and Z coordinate systems. X and Y dimensions pertain to the field of view (FOV) area captured by the ultrasound scan and Z pertains to the axial imaging depth. Only 10 eyes were manually segmented as training data for the DL model and the demographics for these eyes are shown in **Table 1.**

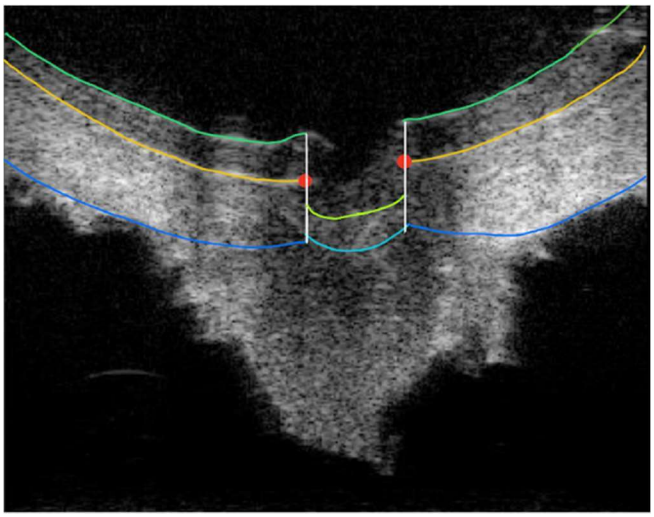

Figure 4: Fully Segmented B-Mode image. Includes Internal Limiting Membrane (Green), Anterior Scleral Boundary Left and Right (Yellow), Poster Sclera Boundary Left and Right (blue), Anterior Lamina Cribrosa (light green), Posterior Lamina Cribrosa (light blue), and Bruch's Membrane Opening (2 Red Points)

After acquiring the 3-D point cloud for the 10 eyes, the data was imported into MatLab for interpolation. Each layers 3-D points were interpolated along a 3-D mesh grid using cubic spline. This method is most precise for data sampled at irregular intervals and for a curved surface, particularly the spherical shape of that of the human eye. Addition to interpolation, a binary smoothing function was applied with a grid size of 30 X 30 along each surface. After all surfaces

have been interpolated and smoothed, full segmented images were developed. These images were 3 class images where the retinal, scleral, and LC layers all had a unique pixel value associated with them. At the end, the ONH was extruded through all layers of the eye separating the retina and sclera into left and right regions. Due to the the radial slices being automatically created when images were loaded into the software for segmentation, both the segmented images and raw images still needed to manually be converted to radial images using imageJ as the custom software did not save the segmentation as radial coordinates. Finally, the 3 class segmented radial images were then separated into binary class images by separating the 3 class image into 3 individual binary images for the retina, sclera, and LC ground truth masks with image dimensions of 342 X 304.

Training the Deep Learning based segmentation model

PyTorch is an open-source DL framework that was used for the development of the DL model. The model architecture used was DeepLabV3+ and the encoder used was Timm-EfficientNet-b0 as these frameworks demonstrated the highest performance in prior lab projects and are commonly used for image segmentation applications.

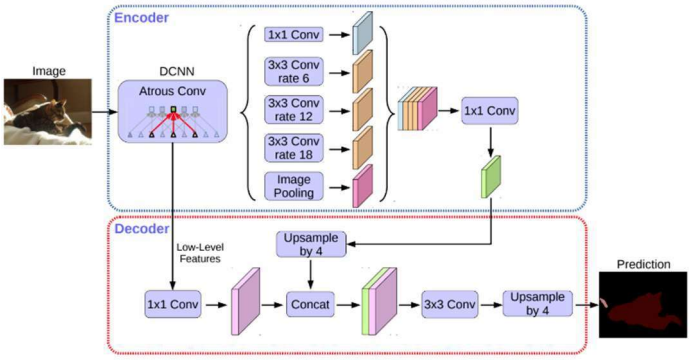

Figure 5: Model Architecture of DeepLab V3+

These models consisting of both convolutional layers and fully connected layers have demonstrated excellent extraction and classification results and production of a segmented image [9]. The model also used the Adam optimizer with a learning rate (LR) of 1E-3. L2 regularization was also applied to this model with alpha values of 1E-5, 1E-4, and 1E-3 as hyperparameters. The value that led to greatest model performance was 1E-5 and this was used for the final segmentation outputs. The model was run 3 different times for each layer class where the ground truth masks of the 10 eyes (n = 800) were trained on and predicted binary masks were outputted. A random 65% training 35% testing split between the total 800 frames was used in which 530 frames were used for actual training and 270 were for evaluation and optimization of hyperparameters. This model was then used to auto segmented the remaining 27 eyes (n = 2160 frames). Model performance was assessed using the pixel-wise binary classification sensitivity, specificity, accuracy, and Dice score. These values are defined in figure 7 below where TP is true positive pixels, TN is true negative pixels, FP is false positive pixels, and FN is false negative pixels.

Figure 6: Producing segmented data from B-Mode slice and how the DL model segments each class. The model outputs a soft segmented image for each layer class

Right Eyes	7
Left Eyes	3
Male	5
Female	4
Healthy	6
Glaucoma	3
African American	3
Caucasian	6
Age Range	20-80
Age Mean	57.1

Table 2: Training Data Demographic Breakdown

$$Dice = \frac{2TP}{2TP + FP + FN}$$

$$Sensitivity = \frac{TP}{TP + FN}$$

$$Specificity = \frac{TN}{TN + FP}$$

$$Accuracy = \frac{TP + TN}{TP + TN + FP + FN}$$

Figure 7: Performance metric calculations of DL model

5.2 Calculating morphological properties using segmented data

Calculating morphological data

Segmented binary masks from each of the 3 layer classes were then loaded into MatLab for thickness calculations. Due to high inaccuracies of LC mask prediction, only the manually segmented data for LC was considered for both the thickness calculations and BMO to LC depth. Additionally, 2 segmented eyes predicted by the DL network were not used for data analysis due to high error in predicted masks. As a result, the total number of eyes used for statistical in

analysis is as follows: Retina: 35, PPS: 37, LC: 10. 2 types of thickness were calculated for each layer which were the axial depth and true thickness. Axial depth is defined as the vertical distance between the top and bottom layers and true thickness is the distance of the shortest line connecting 2 points on the top and bottom layers. These thicknesses were calculated by determining the pixel indices of the top and bottommost layers. Then for each pixel in the top boundary, the total number of pixels were counted vertically between top and bottom layers for vertical thickness and the total number of pixels along the shortest line for the Euclidean thickness. Total pixels were then converted to distance by multiplying by pixel size in terms of microns.

Additionally, BMO to anterior LC depth was also calculated to assess any major posterior deformation of the LC in glaucoma. The BMO points were not marked in Multiview, however, the 2 endpoints of the anterior sclera were used as the BMO left and right points. A line was fitted between the two points and vertical distance at 1/3, ½, and the 2/3 mark of the fitted line were calculated. Once all the data was collected for all the eyes in the study, statistical analysis was used to compare significances between both glaucoma and age groups.

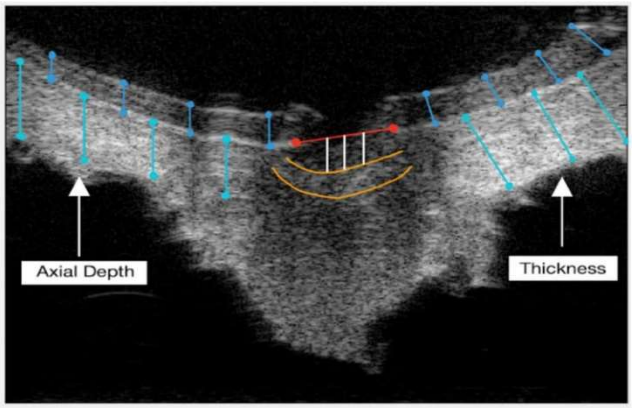

Figure 8: Method for morphological calculations

Statistical analysis

2 sample 2-tailed unpaired T-Tests were performed between each healthy and Glaucoma group for the 3 anatomical layers thickness and only the Euclidean thickness was considered for this analysis. Additionally, a regression analysis was computed for the both the Euclidean and axial thickness of the PPS with age. The correlation coefficient and the significance of the slope were analyzed for non-zero significance. All statistical tests were performed at $\alpha = 0.05$.

6. Results and Discussions

Model performance and optimization was first assessed by comparing the metrics using different coefficients of regularization with data shown in Table 3. Using the optimal value of α = 1E-5, the test set was fed into to the model to compute overall accuracy and error loss for each of the 3 layer classes with the test set.

Layer Type	Sensitivity	Specificity	Accuracy	Dice Score
Retina	0.9275	0.9945	0.9904	0.9224
Sclera	0.9677	0.9838	0.9891	0.9667
LC	0.6829	0.9904	0.9704	0.7252

Table 3: Model performance metrics on test set with $\alpha = 10^{-5}$

The Euclidean thicknesses of retina, PPS, and LC are shown in Figure 9 and only the retina exhibited significant difference between healthy 424.9 and glaucoma 350.9 with a P-value of 0.0019 (**Figure 9)**. For the regression and correlation analysis, the Axial thickness exhibited significant trends with age with correlation value of -0.38 and significant non-zero slope of -2.24 with R-squared value of 0.144 **(Figure 10).**

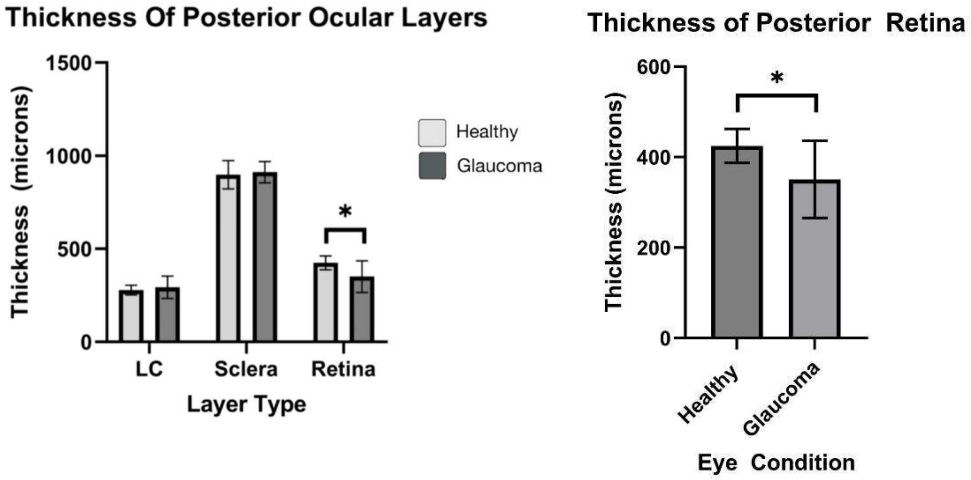

Figure 9: Mean Thickness in each posterior ocular layer between both healthy and glaucoma patients ($\alpha = 0.05$, Asterisk indicates significant)

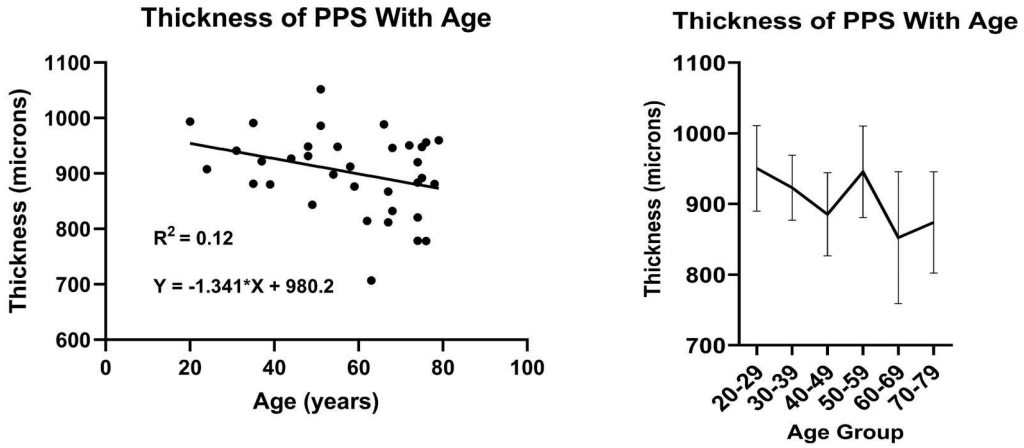

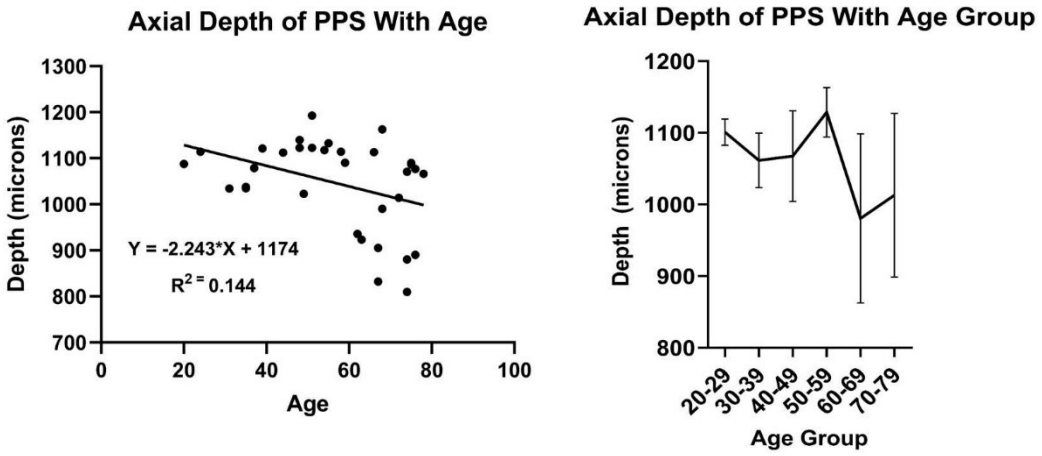

Figure 10: Correlation and regression between PPS thinning and aging. Correlation tests shows significant results with **(R = -0.38, p = 0.026)** with axial definition of thickness (bottom left and right). Regression analysis also yielded a significant non-zero slope value **(p = 0.0296)**

While the means between LC to BMO distance were not statistically significant between glaucoma and healthy groups, there was still a noticeable difference. The mean depth for healthy was 474.2 microns and 545.6 microns for glaucoma **(Figure 11).**

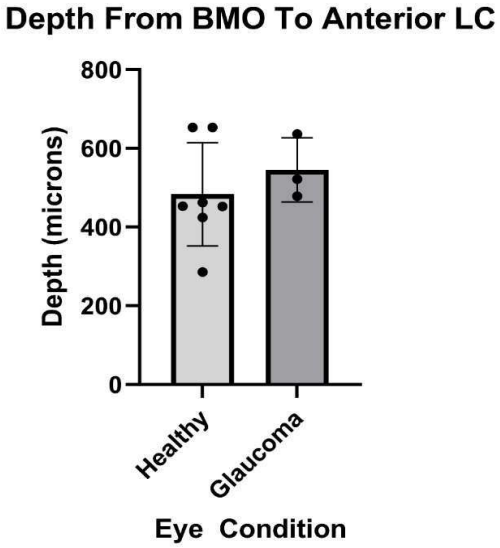

Figure 11: Mean BMO to anterior LC depth between healthy and glaucoma eyes ($\alpha = 0.05$)

Glaucoma results in retinal ganglion cell loss which may explain why the retina was significantly thinner in glaucoma patients compared to healthy eyes. On the other hand, both the PPS and LC are composed mostly of extracellular matrix such as collagen types 1 and 3, as opposed to mostly neural tissue in the retina. The primary purpose of the sclera is to support the shape of the eye and absorb any pressure related damages. The sclera is very stiff due to fiber orientation and is able to hold its shape in elevated IOP levels in Glaucoma. Higher IOP in glaucoma eyes shows the LC could be axially displaced because unlike the sclera, the LC is less stiff and more likely to axially deform. On the other hand, as people age, the PPS and LC biomechanical properties changes and can lead to higher glaucoma risk.

7. Conclusions and Future Work

This study demonstrated feasibility in using Deep Learning to effectively extract information from ultrasound data. Automation in segmentation of the PPS, LC, and retina can be used respectively as all the metrics were seen as greater than 90%. Future research can optimize this model by training on even more diverse patients and performing segmentation on enhanced images as the LC was not well predicted by the model. In many of the images the LC and or sclera boundaries were often not easily traceable. This is primarily due to the low resolution of LC layer in the ultrasound images making both the manual segmented masks and predicted masks very inaccurate. Additionally, further model optimization can be performed such as trying different model architectures and utilizing different regularization methods. A multiclass prediction model can be implemented rather than binary classification to save computational time and power. Diffusion models for image denoising can be implemented to further enhance ultrasound scans.

The significant difference seen in retinal thickness between healthy and Glaucoma eyes shows promising application of the use of DL in automated segmentation as this finding is consistent with previous results. Although the reported healthy retinal thickness was on the thicker end of the spectrum compared to previously reported literature, this can be a result of only considering tissue close to the ONH and not the entire posterior surface. Although the PPS thickness was not significantly different between healthy and glaucoma eyes, one limitation of the analysis was that a wider age range was used for the data set in the healthy group consisting of patients with ages 20-70 years old while the glaucoma group was only in the range of 70-80 years old. Future analysis can do comparisons of thickness within the same age range to mitigate any confounding effects. Similarly, the thinning of the PPS with age is yet again consistent with previous findings further validating the DL segmentation model of accurate thickness calculations.

Although further research is necessary, current data demonstrating the age-related changes in the sclera demonstrate the power of ultrasonic imaging and automated segmentation in glaucoma early detection. Thus, this study is the first step in using auto segmented images in characterizing age related morphological differences with the hopes of developing more advanced diagnosis of glaucoma involving sclera and LC morphometric parameters.

References

[1] *The Macular Thickness and Volume in Glaucoma: An ... - Wiley Online Library*. https://onlinelibrary.wiley.com/doi/full/10.1034/j.1600-0420.80.s236.44.x.

[2] "Glaucoma: Facts & Figures." *Glaucoma: Facts & Figures | BrightFocus Foundation*, https://www.brightfocus.org/glaucoma/article/glaucoma-facts-figures#:~:text=Glaucoma%20is%20a%20leading%20cause,United%20States%20and%20the%20world.&text=More%20than%20three%20million%20Americans,form%2C%20open%2Dangle%20glaucoma.

[3] "Glaucoma Tests: What to Expect & How to Interpret Results." *Cleveland Clinic*, https://my.clevelandclinic.org/health/diagnostics/22514-glaucoma-tests#:~:text=Your%20ophthalmologist%20uses%20eye%20drops,test%20is%20also%20called%20gonioscop.

[4] Sher, Ifat, et al. "*In Vivo* Retinal Imaging in Translational Regenerative Research." *Annals of Translational Medicine*, U.S. National Library of Medicine, Sept. 2020, https://www.ncbi.nlm.nih.gov/pmc/articles/PMC7575995/.

[5] "Glaucoma." *Mayo Clinic*, Mayo Foundation for Medical Education and Research, 30 Sept. 2022, https://www.mayoclinic.org/diseases-conditions/glaucoma/symptoms-causes/syc-20372839#:~:text=Glaucoma%20develops%20when%20the%20optic,increased%20pressure%20in%20the%20eye.

[6] Downs, J Crawford, et al. "Mechanical Environment of the Optic Nerve Head in Glaucoma." *Optometry and Vision Science : Official Publication of the American Academy of Optometry*, U.S. National Library of Medicine, June 2008, https://www.ncbi.nlm.nih.gov/pmc/articles/PMC2714589/.

[7] "Glaucoma: Causes, Types, Symptoms, Diagnosis, and Treatment." *WebMD*, WebMD, https://www.webmd.com/eye-health/glaucoma-eyes.

[8] Grzybowski, Andrzej, et al. "Primary Open Angle Glaucoma and Vascular Risk Factors: A Review of Population Based Studies from 1990 to 2019." *Journal of Clinical Medicine*, U.S. National Library of Medicine, 11 Mar. 2020, https://www.ncbi.nlm.nih.gov/pmc/articles/PMC7141380/.

[9] (JCD, Ocular Biomechanics Laboratory. "Mechanical Environment of the Optic Nerve Head in Glaucoma : Optometry and Vision Science." *LWW*, https://journals.lww.com/optvissci/Abstract/2008/06000/Mechanical_Environment_of_the_Optic_Nerve_Head_in.13.aspx.

[10] Wang, Shanshan, et al. "Recent Advances in Applications of Multimodal Ultrasound-Guided Photoacoustic Imaging Technology." *Visual Computing for Industry, Biomedicine,*

and Art, U.S. National Library of Medicine, 21 Oct. 2020, https://www.ncbi.nlm.nih.gov/pmc/articles/PMC7575676/.

[11] Downs, J Crawford, and Christopher A Girkin. "Lamina Cribrosa in Glaucoma." *Current Opinion in Ophthalmology*, U.S. National Library of Medicine, Mar. 2017, https://www.ncbi.nlm.nih.gov/pmc/articles/PMC5480216/.

[12] Hua, Rui, et al. "Detection of Preperimetric Glaucoma Using Bruch Membrane Opening, Neural Canal and Posterior Pole Asymmetry Analysis of Optical Coherence Tomography." *Nature News*, Nature Publishing Group, 17 Feb. 2016, https://www.nature.com/articles/srep21743.

[13] Andrew J. Tatham FRCOphth, et al. "Detecting Structural Progression in Glaucoma with Optical Coherence Tomography." *Ophthalmology*, Elsevier, 17 Nov. 2017, https://www.sciencedirect.com/science/article/pii/S0161642017305146?casa_token=jkEXt_ZoRyIAAAAA%3ACNiZfgWWMZoqyL5SBobqCyksgqI8jyaqe8DQE8yxuPeIZ_ADEptfy4e4c0F-qAGcDmGqk2Jv-g.

[14] Clayson, Keyton, et al. "Ocular Pulse Elastography: Imaging Corneal Biomechanical Responses to Simulated Ocular Pulse Using Ultrasound." *Translational Vision Science & Technology*, The Association for Research in Vision and Ophthalmology, 28 Jan. 2020, https://tvst.arvojournals.org/article.aspx?articleid=2760476.

[15] Vidal-Sanz, Manuel, et al. "Retinal Neurodegeneration in Experimental Glaucoma." *Progress in brain research*, 2015, pp. 1–35. https://doi.org/10.1016/bs.pbr.2015.04.008.

[16] *Normal Tension Glaucoma - EyeWiki*. 10 Feb. 2024, eyewiki.aao.org/Normal_Tension_Glaucoma#:~:text=Establishment%20of%20these%20norms%20has,untreated%20IOP%20of%20%3C22%20mmHg.